



INNSPUB

RESEARCH PAPER

**Journal of Biodiversity and Environmental Sciences (JBES)**

ISSN: 2220-6663 (Print) 2222-3045 (Online)

Vol. 6, No. 4, p. 552-561, 2015

<http://www.innspub.net>**OPEN ACCESS**

## Fabrication of perovskite-type oxide nanopowders as a novel adsorbent in removal of Bromo Thymol Blue dye from aqueous solutions

Zohreh Zaman, Haman Tavakkoli\*

*Department of Chemistry, College of Science, Ahvaz Branch, Islamic Azad University, Ahvaz, Iran*

Article published on April 30, 2015

**Key words:** Nanopowder, Perovskite-type oxide, Bromo thymol blue, Isotherm.

### Abstract

Nanoparticles of perovskite-type  $Gd_{0.5}Ca_{0.5}CrO_3$  was investigated for its ability to perform as a suitable sorbent for anionic dye from aqueous solution. The nanoperovskite were characterized using X-ray powder diffraction (XRD), Fourier transform infrared spectroscopy (FTIR) and scanning electron microscopy (SEM). The effects of various experimental factors; adsorbent dose, contact time, pH and dye concentration were studied by using the batch technique. Experimental results indicate that the prepared  $Gd_{0.5}Ca_{0.5}CrO_3$  nanopowder can remove 91.38% of BTB dye under optimum operational conditions of a dosage of 0.02 g, pH 2, contact time of 25 min and initial dye concentration of 50mg/L. Adsorption isotherms have been modeled by Langmuir, Freundlich, Temkin and Dubinin-Radushkevich (D-R). The Langmuir model displayed the best fit for the isothermal data. The maximum predicted adsorption capacities were 300 mg/g for Bromo Thymol Blue (BTB) dye. The results showed that the sorption kinetics of BTB removal from aqueous solutions onto nanopowder fitted well with the pseudo-second-order model.

\*Corresponding Author: Haman Tavakkoli ✉ [htavakkoli59@gmail.com](mailto:htavakkoli59@gmail.com)

## Introduction

The family of perovskite-type oxides generally formulated as  $ABO_3$  (A is a rare earth metal with large ionic radius or alkali earth metals; B is a transition metal with a small ionic radius) Significant catalytic applications of these perovskites include reactors for partial and total oxidation of hydrocarbons and in devices for the removal of pollutants from combustion gases (Tejuca *et al.*, 1993; Schaak *et al.*, 2002) and could be considered as an adsorbent /catalyst material for the removal of dyes (Jeong *et al.*, 2006; Carbajo *et al.*, 2006).

Dye effluents from textile industries and photographic industries are becoming a serious environmental problem because of their toxicity, unacceptable color, high chemical oxygen demand content, and biological degradation (Siddique *et al.*, 2009). Dyes can be classified as anionic (direct, acid, and reactive dyes), cationic (basic dyes) and non-ionic (disperse dyes) (Mishra and Tripathy, 1993). Waste waters offer considerable resistance for their biodegradation due to presence of these heat and light stable dyes, thus upsetting aquatic life (Wong and Yu, 1993). Several treatment methods including coagulation, chemical oxidation, membrane separation and adsorption techniques have been proposed for the treatment of dye waste water. Considerable amounts of the literature reports the adsorption of dyes on various adsorbent surfaces especially nanomaterials (Yazdambakhsh *et al.*, 2010; Wu *et al.*, 2004).

The first aim of the present study is to fabricate and characterize of perovskite-type oxide nanoparticles  $Gd_{0.5}Ca_{0.5}CrO_3$ . Investigation of the efficiency of the perovskite-type oxide nanoparticles as adsorbent for the removal of Bromo Thymol Blue dye (BTB), from aqueous solutions is the second goal and to explain the adsorption of BTB onto nanoparticles  $Gd_{0.5}Ca_{0.5}CrO_3$  using isotherm models.

## Material and methods

### Reagents

The chemicals and reagents used in this work include  $Gd(NO_3)_3 \cdot 6H_2O$  (99.9%),  $Ca(NO_3)_2 \cdot 4H_2O$  (99.9%) and  $Cr(NO_3)_3 \cdot 9H_2O$  (99.9%) obtained from Merck, Germany; citric acid (CA) (99.5% purity), was purchased from Aldrich, USA. 2.1. The chemical structures of Bromo Thymol Blue (BTB) dye is given in Fig. 1.

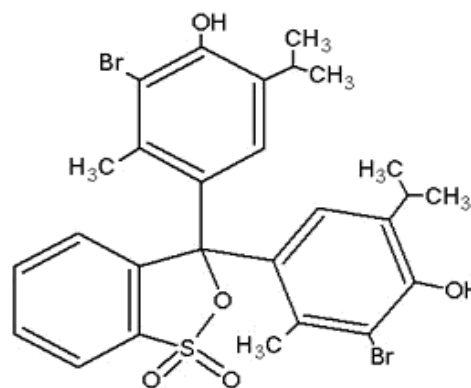


**Fig. 1.** Molecular structures of Bromo Thymol Blue (BTB) dye.

### Preparation of $Gd_{0.5}Ca_{0.5}CrO_3$ powders

For preparing the nanoperovskite  $Gd_{0.5}Ca_{0.5}CrO_3$ , proportional amounts of  $Gd(NO_3)_3 \cdot 6H_2O$ ,  $Ca(NO_3)_2 \cdot 4H_2O$ , and  $Cr(NO_3)_3 \cdot 9H_2O$  were dissolved in 40 ml of deionized water. Then, citric acid (CA) was added to the metal solution by stirring at room temperature. The solution was refluxed with stirring for 90 min to convert it to a stable complex. The gel was heated at  $80^\circ C$  for 3 h and then dried at  $112^\circ C$  for 19 h. It was grounded in an agate mortar to change into a powder and calcinated at  $700^\circ C$  in air for 8 h.

### Characterization methods

The dried powders were analyzed by Fourier transform infrared spectroscopy using thermo Nicolet Nexus 870 FTIR spectrometer. The crystallization and microstructure of the oxide powders were characterized with XRD in a  $2\theta$  range from  $20$  to  $80^\circ$ , using  $CuK\alpha$  radiation ( $\lambda = 1.5418 \text{ \AA}$ ) on a Rigaku D/MAX RB XRD diffractometer equipped with a curved graphite monochromator. A scanning electron microscope (SEM, LEO1450 VP,  $V = 26 \text{ kV}$ ) was used to study the morphology of the calcined powders.

*Dye removal experiments*

Dye adsorption by the GCCO nanopowder was determined in batch experiments at different contact times (2–30 min), dye concentrations (50–300 mg/L), different doses of adsorbent (0.005–0.02 g) and pH of solution (1–12). The initial dye solution concentration for all batch experiments was adjusted to 50 mg/L except for the experiments in which the effect of the initial dye concentration was tested. All experiments were conducted at 25 °C.

**Results and discussion**

*FT-IR studies*

Figure 2a and b shows the FT-IR spectra of the dry gel before calcination and calcined powder at 700 °C for 8 h, respectively. As shown in Fig. 2a, the broad absorption band around 3415 cm<sup>-1</sup> corresponds to the ν<sub>O-H</sub> stretching vibrations of water molecules (Kuznetsov *et al.*, 2002) and characteristic bands at about 1226 and 1384 cm<sup>-1</sup> corresponds to the stretching mode of M–O–C group (Kuznetsov *et al.*, 2002, Kim and Honma, 2004) and the anti-symmetric ν<sub>NO<sub>2</sub><sup>-</sup></sub> stretching vibration (Liu *et al.*, 2007), respectively. The absorption band around 1081 cm<sup>-1</sup> is assigned to C–O bond (Nakamoto, 1978). In the FT-IR spectrum of the GCCO nanopowder (Fig. 2b) a strong peak appears at 590 cm<sup>-1</sup>, which is assigned to the M–O bond.

*X-ray diffraction studies*

Fig.3 shows the XRD patterns of the GCCO nanopowder prepared by sol–gel method. The diffractograms reveal that the crystalline perovskite structure is the main phase for synthesized nanopowder. The most intense diffraction peak (2θ = 32.58) is a single peak for all of the studied perovskites (Merino *et al.*, 2006). The crystalline sizes of the GCCO nanopowder were determined by means of an X-ray line-broadening method using the Scherrer equation:

$$D_{hkl} = \frac{0.9\lambda}{\beta_{hkl} \cos \theta_{hkl}}$$

Where D<sub>hkl</sub> is the particle size in nanometers, λ is the wavelength of the radiation (1.54056 Å for CuK<sub>α</sub> radiation), k is a constant equal to 0.9, β<sub>hkl</sub> is the peak width at half-maximum intensity and θ is the peak position. The crystalline size of the GCCO nanopowder calcined at temperature of 700 °C was found to be 30 nm.

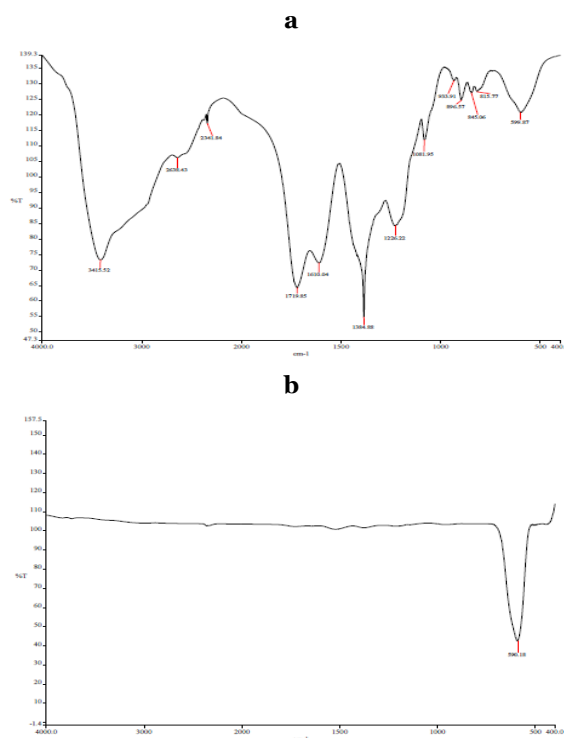


**Fig. 2.** (a) FT-IR spectra of the GCCO dry gel before calcinations. (b) FT-IR spectra of the calcined powders at 700° C.

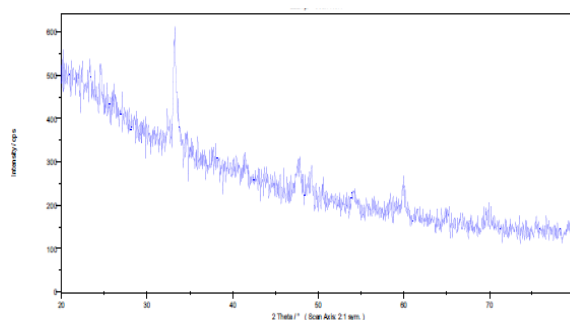


**Fig. 3.** The XRD patterns of the GCCO nanoparticles at 700 °C.

*Microscopic analyses*

Scanning electron microscopy (SEM) of the GCCO nanoparticles prepared by the sol–gel method is

shown in Fig. 4. This image exhibits typical morphologies for prepared powder. Based on the SEM images, porosity of the surface is evident and it seems that the particles have not grown with uniform size. The particles size of GCCO that were propagated on the surface seems to be in the range of 29–97 nm.

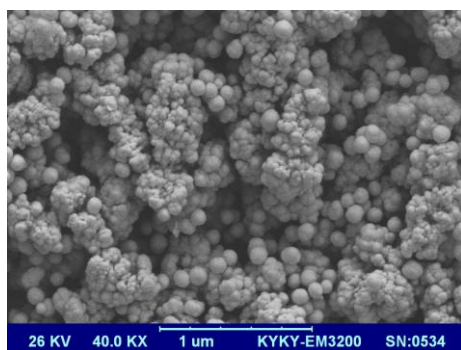


Fig. 4. SEM images of GCCO nanoparticles.

*Effects of various conditions on adsorption*

*The Effect of pH on dye adsorption*

One of the most important factors in adsorption studies is the effect of acidity on the medium (Calvete *et al.*, 2010). Different species may present divergent ranges of suitable pH depending on which adsorbent is used. The effect of initial pH on the adsorption capacity of BTB dye using GCCO adsorbent was evaluated within pH range between 1 and 12 with a stirring time of 25 min. The initial concentrations of dye and adsorbent dosage were set at 50 mg/L and 0.02 g, respectively. The percentage of dye removal is defined as:

$$\text{Removal rate \%} = \frac{C_0 - C_e}{C_0} \times 100$$

where  $C_0$  and  $C_e$  represent the initial and equilibrium concentrations of dye at given time, respectively. Fig. 5 shows that the effect of pH on the adsorptive removal of BTB by GCCO nanopowder. The percentage removal of BTB (anionic dye) was maximum at acidic pH (pH 2) and decreased with further increase in pH. BTB dye is an acidic dye that has negative charge in solution, which favors electrostatic interactions between the GCCO surface and dye molecules leading to the strong adsorption. Therefore, to have the optimized condition to remove

BTB, acidic pH should be applied and pH 2 seems to lead to the best result; so this pH was selected to run further experiments.

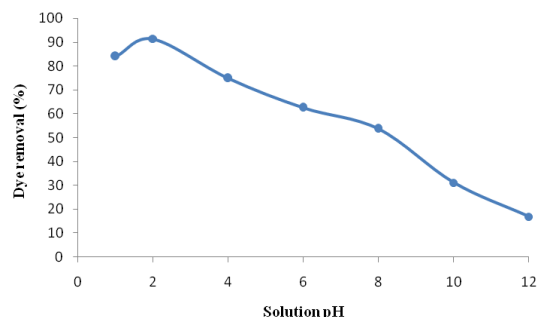


Fig. 5. Effect of pH on the removal of dye by GCCO nanopowder (contact time = 25 min, initial dye concentration = 50mg/L, GCCO dosage: 0.02 g).

*Effect of adsorbent amounts and contact time*

By increasing amounts of GCCO nanopowder, the removal efficiency increased due to increase in the accessible sites for the adsorption of the analyte. Fig. 6 shows that the removal efficiency of BTB dye with the initial dosage of 0.005g, increased from 63.40 % at the second minute of contact to 87.33% at time equals to 30 min by keeping constant stirring, however, with increasing GCCO dosage to 0.02 g, obtained removal efficiency in the second minute of stirring was 86.46%, and in the 25 minute of stirring was 91.38%. In addition, increasing the contact time from 2 to 30 min with different dosages of adsorbents led to decreasing in the concentration of BTB dye.

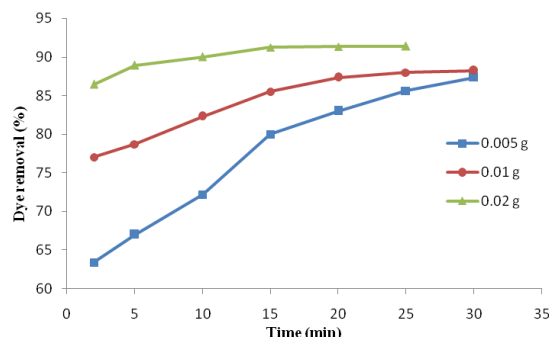
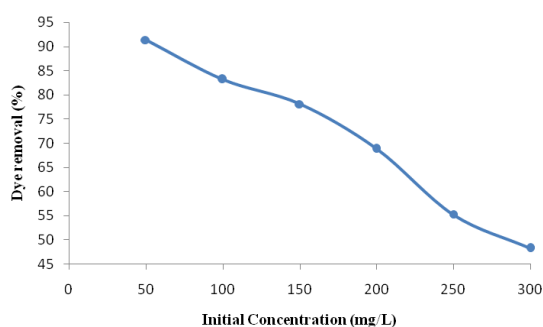


Fig. 6. Effect of stirring time on removal of dye in different doses (■) 0.005 g, (●) 0.01 g, (▲) 0.02 g of GCCO (initial dye concentration=50 mg/L, initial pH = 2).

*Effect of dye concentration*

The initial dye concentration is another important variable that can affect the adsorption process. The effect of initial BTB concentration on dye removal efficiency by GCCO nanoparticles was studied by varying the initial dye concentration from 50 to 300 mg/L at pH 2, a catalyst dosage of 0.02 g and contact time of 25 min, as shown in Fig. 7. Results show that removal of textile dye BTB decreases with increasing initial concentration. As it is obvious, the percentage removal of BTB decreased from around 91.38% at a concentration of 50 mg/L to 48.28% when the concentration was increased to 300 mg/L. This behavior reveals the dependency of adsorption to initial concentration of BTB.



**Fig. 7.** Effect of initial adsorbate concentration of on removal of dye by GCCO nanopowder (contact time = 25 min, GCCO dosage = 0.02 g, pH = 2).

*Adsorption isotherms*

The equilibrium isotherm of a specific adsorbent represents its adsorptive characteristics and analysis of isotherm data is so important to predict the adsorption capacity of the adsorbent, which is one of the main parameters required for designing the adsorption processes (Afkhami and Moosavi, 2010).

The amount of dye adsorbed onto GCCO nanoparticles has been calculated based on the following mass balance equation:

$$q_e = \frac{V(C_0 - C_e)}{m}$$

Where  $q_e$  was the equilibrium adsorption capacity of dye adsorbed on unit mass of nanoparticles (mg/g),  $V$  is the volume of the dye solution (L),  $C_0$  and  $C_e$  were

the initial dye concentration (mg/L) and dye concentration (mg/L) at equilibrium and  $m$ (g) is the mass of dry GCCO nanoparticles added.

Analysis of the equilibrium data is important to develop an equation which accurately represents the results and which could be used for design purposes. The equilibrium adsorption data of BTB dye onto GCCO adsorbent was analyzed by the use of well known models given by the Langmuir, Freundlich, Temkin and Dubinin–Radushkevich, isotherm models.

*Langmuir isotherm model*

In its formulation, this empirical model assumes monolayer adsorption (the adsorbed layer is one molecule in thickness), with adsorption can only occur at a finite (fixed) number of definite localized sites, that are identical and equivalent, with no lateral interaction and steric hindrance between the adsorbed molecules, even on adjacent sites (Vijayaraghavan *et al.*, 2006). In its derivation, Langmuir isotherm refers to homogeneous adsorption, which each molecule possess constant enthalpies and sorption activation energy (all sites possess equal affinity for the adsorbate) (Kundu and Gupta, 2006), can be represented as follows:

$$\frac{C_e}{q_e} = \frac{1}{bq_{max}} + \frac{C_e}{q_{max}}$$

where the  $q_{max}$  (mg/g) is the surface concentration at monolayer coverage which illustrates the maximum value of  $q_e$  and it can be attained as  $C_e$  is increased. The values of  $q_{max}$  and  $b$  can be determined from the linear regression plot of  $(C_e/q_e)$  versus  $C_e$ .

*Freundlich isotherm model*

Freundlich isotherm is the earliest known relationship describing the non-ideal and reversible adsorption, not restricted to the formation of monolayer (Freundlich, 1906). This empirical model can be applied to multilayer adsorption, with non-uniform distribution of adsorption heat and affinities over the heterogeneous surface (Adamson and Gast, 1997). The linearized equation is expressed as:

$$\log q_{\varepsilon} = \log K_F + \frac{1}{n} \log C_{\varepsilon}$$

where  $K_F$  and  $n$  are constants of the Freundlich equation. The constant  $K_F$  represents the capacity of the adsorbent for the adsorbate and  $n$  is related to the adsorption distribution.

*Temkin isotherm model*

The Temkin isotherm equation assumes that the heat of adsorption of all the molecules in layer decreases linearly with coverage due to adsorbent-adsorbate interactions, and that the adsorption is characterized by a uniform distribution of the bonding energies, up to some maximum binding energy (Temkin and Pyzhev, 1940). The Temkin isotherm is represented by the following equation:

$$q_{\varepsilon} = \frac{RT}{b_T} \ln A_T + \frac{RT}{b_T} \ln C_{\varepsilon}$$

Where,  $T$  is the absolute temperature (K),  $R$  is the universal gas constant (8.314 J/mol. K),  $A_T$  is the equilibrium binding constant (L/g),  $b_T$  is the variation of adsorption energy (J/mol).

*Dubinin–Radushkevich isotherm model*

Dubinin–Radushkevich isotherm (Dubinin and Radushkevich, 1947), is an empirical model initially conceived for the adsorption of subcritical vapors on to micropore solids following a pore filling mechanism. It is generally applied to express the adsorption mechanism (Gunay *et al.*, 2007) with a Gaussian energy distribution onto a heterogeneous surface (Dabrowski, 2001). The Dubinin–Radushkevich isotherm is represented by the following equation:

$$\ln q_{\varepsilon} = \ln q_{max} - K\varepsilon^2$$

$K$  is Dubinin–Radushkevich isotherm constant ( $\text{mol}^2/\text{kJ}^2$ ),  $\varepsilon$  is the Polanyi potential.

The parameter  $\varepsilon$  can be correlated as:

$$\varepsilon = RT \ln \left[ 1 + \frac{1}{C_{\varepsilon}} \right]$$

The mean adsorption energy,  $E$  (kJ/mol) is calculated with the help of following equation:

$$E = \frac{1}{\sqrt{2K}}$$

where  $R$ ,  $T$  and  $C_e$  represent the gas constant (8.314 J/mol. K), absolute temperature (K) and adsorbate equilibrium concentration (mg/L), respectively.

The obtained experimental data were fit with Langmuir, Freundlich, Temkin and Dubinin–Radushkevich models; the resulting plots are shown in Fig. 8. Table 1 summarizes the models constants and the determination coefficients. The  $R^2$  values for the Langmuir model are closer to unity than those for the other isotherm models for GCCO nanopowder ( $R^2 = 0.994$ ). The Langmuir isotherm equation is therefore expected to best represent the equilibrium adsorption data. This indicates that the adsorption of BTB on GCCO nanoparticles is better described by the Langmuir model. This in turn suggests that adsorption occurs as the monolayer dyes adsorb on to the homogenous adsorbent surface. Due to the steric hindrance associated with the size of the dyes, a higher adsorption capacity can be achieved for small dye molecules (Jindarom *et al.*, 2007) under the same experimental conditions.

**Table 1.** Isotherm parameters for removal of BTB dye onto GCCO nanopowder.

Langmuir constants		
$q_{max}$ (mg.g <sup>-1</sup> )	$b$ (L.mg <sup>-1</sup> )	$R^2$
300	0.013	0.994
Freundlich constants		
$1/n$	$K_F((\text{mg/g})(\text{L/mg})^{1/n})$	$R^2$
0.665	12.50	0.989
Temkin constants		
$A_T$ (L/g)	$b_T$ (j/mol)	$R^2$
0.223	34.40	0.976
(D-R) constants		
$q_{max}$ (mg.g <sup>-1</sup> )	$E$ (KJ.mol <sup>-1</sup> )	$R^2$
161.09	2.01	0.809

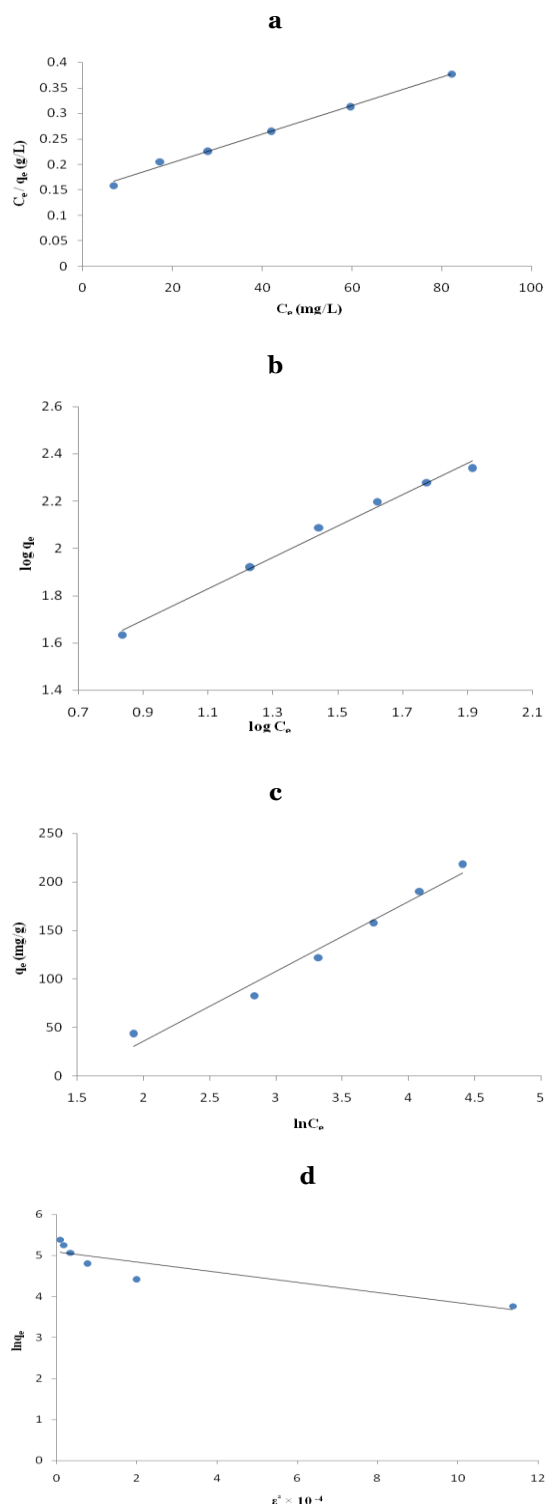


**Fig. 8.** Isotherm plots of BTB dye adsorption onto GCCO nanopowders: (a) Langmuir isotherm, (b) Freundlich isotherm, (c) Temkin isotherm and (d) Dubinin–Radushkevich isotherm (Experimental conditions: pH= 2; GCCO dosage = 0.02 g; initial dye concentration = 50, 100, 150, 200, 250, 300 mg/L and contact time = 25 min).

The favorability of the BTB dye adsorption process onto GCCO nanopowder was evaluated using a dimensionless parameter ( $R_L$ ) derived from the Langmuir expression. It is defined as follows:

$$R_L = \frac{1}{1 + bC_0}$$

where  $b$  is the Langmuir constant and  $C_0$  is the highest initial dye concentration (mg/L). The adsorption process can be defined as irreversible ( $R_L = 0$ ), favorable ( $0 < R_L < 1$ ), linear ( $R_L = 1$ ) or unfavorable ( $R_L > 1$ ) in terms of  $R_L$  (Sivaraj *et al.*, 2001). The calculated values of  $R_L$  for adsorption of BTB dye fall between 0 and 1, hence the adsorption of BTB onto GCCO adsorbent is favorable.

#### Adsorption kinetics

Several models are available to investigate the adsorption kinetics. In order to investigate the adsorption processes of BTB on GCCO nanopowder, two kinetic models were used, including pseudo-first-order and pseudo-second-order reaction rate equations are the most commonly applied models (Bayramoglu *et al.*, 2006; Hsueh *et al.*, 2007).

The pseudo-first-order equations expressed as follows:

$$\ln (q_e - q_t) = \ln q_e - K_1 t$$

The pseudo-first-order equation is:

$$\frac{t}{q_t} = \frac{1}{K_2 q_e^2} + \frac{t}{q_e}$$

Where  $k_1$  and  $k_2$  are constants of adsorption rate,  $q_t$  is adsorption capacity at time  $t$ ,  $q_e$  is adsorption capacity at equilibrium condition.

To describe the adsorption behavior and rate, the data obtained from adsorption kinetic experiments were evaluated using pseudo-first-order and pseudo-second-order reaction rate models. Plots of experimental results of dye fitted to the selected adsorption models are shown in Fig. 9. The kinetic constants along with the correlation coefficients are listed in Table 2. As shown in Table 2, higher values

of  $R^2$  were obtained for pseudo-second-order, indicating that the adsorption rates of BTB dye onto the GCCO nanopowder can be appropriately described using the pseudo-second-order kinetics.

**Table 2.** Kinetic parameters for the removal of BTB dye onto GCCO nanopowder.

Pseudo-first-order constants		
$q_e$ (mg/g)	$K_1$ (min <sup>-1</sup> )	$R^2$
10.91	0.124	0.974
Pseudo-second-order constants		
$q_e$ (mg/g)	$k_2$ (g/(mg.min))	$R^2$
47.61	0.028	0.999

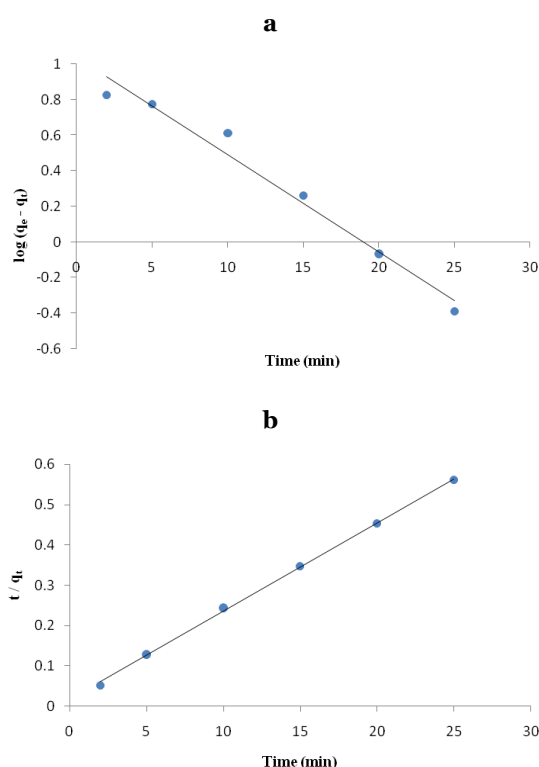


**Fig. 9.** Plots of first and second-order rates for adsorption of BTB dye onto GCCO nanopowders: (a) pseudo-first-order rate and (b) pseudo-second-order rate.

**Conclusions**

In summary, nanoparticles  $Gd_{0.5}Ca_{0.5}CrO_3$  have been fabricated by sol-gel method. The FTIR spectroscopy confirmed the structure of obtained nanoparticles.

The XRD reveal that the GCCO nanoparticles prepared by calcinating the gel precursor at 700 °c for 8 h have good crystallinity in perovskite structure. The SEM images show regular morphology and particle size distribution on the surface. In the present study, we demonstrated the perovskite nanoparticles can act as novel adsorbent materials for degradation of BTB dye. The results demonstrated that the BTB dye can be successfully removed from aqueous solutions by the new GCCO nanoparticles. Isotherm modeling showed that Langmuir isotherm best-fits equilibrium data for BTB-GCCO system. The sorption kinetic can be successfully describes by a pseudo-second-order equation for the removal of BTB on GCCO nanoparticles.

**References**

**Adamson AW, Gast AP.** 1997. Physical Chemistry of Surfaces, sixth ed., Wiley- Interscience, New York.

**Afkhami A, Moosavi R.** 2010. Adsorptive removal of Congo red, a carcinogenic textile dye, from aqueous solutions by magnetite nanoparticles. Journal of Hazardous Materials **174**, 398–403.

**Bayramoglu G, Celik G, Arica MY.** 2006. Biosorption of Reactive Blue 4 dye by native and treated fungus phanerocheatechrysosporium: Batch and continuous flow system studies, B **137**, 1689–1697.

**Calvete T, Lima EC, Cardoso NF, Vaghetti JCP, Dias SLP, Pavan FA.** 2010. Application of carbon adsorbents prepared from the Brazilian-pine fruit shell for removal of reactive orange 16 from aqueous solution – kinetic, equilibrium, and thermodynamic studies. Chemical Engineering Journal **91**, 1695–1706.

**Carbajo M, Beltran FJ, Medina F, Gimeno O, Rivas FJ.** 2006. Catalytic ozonation of phenolic compounds: the case of gallic acid. Applied Catalysis B: Environmental **67**, 177–186.

- Dabrowski A.** 2001. Adsorption—from theory to practice. *Advances in Colloid and Interface Science* **93**, 135–224.
- Dubin M, Radushkevich LV.** 1947. The equation of the characteristic curve of the activated charcoal. *Proceedings Academy Sciences USSR Physical Chemistry Section* **55**, 331–337.
- Freundlich HMF.** 1906. Over the adsorption in solution. *Z Physics Chemistry A* **57**, 385–471.
- Gunay A, Arslankaya E, Tosun I.** 2007. Lead removal from aqueous solution by natural and pretreated clinoptilolite: adsorption equilibrium and kinetics. *Journal of Hazardous Materials* **146**, 362–371.
- Hsueh CL, Lu YW, Hung CC, Huang YH, Chen CY.** 2007. Removal of Orange-G and Methyl Violet dyes by adsorption onto bagasse fly ash-kinetic study and equilibrium isotherm analyses. *Dyes and Pigments* **75**, 130–135.
- Jeong H, Kim T, Kim D, Kim K.** 2006. Hydrogen production by the photocatalytic over all water splitting on NiO/Sr<sub>3</sub>Ti<sub>2</sub>O<sub>7</sub>: effect of preparation method. *International Journal of Hydrogen Energy* **31**, 1142–1146.
- Jindarom C, Meeyoo V, Kitiyanan B, Rirksomboon T, Rangsunvigit P.** 2007. Surface characterization and dye adsorptive capacities of char obtained from pyrolysis/gasification of sewage sludge. *Chemical Engineering Journal* **133**, 239–246.
- Kim J, Honma I.** 2004. Synthesis and proton conducting properties of zirconia bridged hydrocarbon /phosphotungstic acid hybrid materials. *Electrochimica Acta* **49**, 3179–3183.
- Kundu S, Gupta AK.** 2006. Arsenic adsorption onto iron oxide-coated cement (IOCC): regression analysis of equilibrium data with several isotherm models and their optimization. *Chemical Engineering Journal* **122**, 93–106.
- Kuznetsov PN, Kuznetzova LI, Zhyzhaev AM, Pashkov GL, Boldyrev VV.** 2002. Ultra fast synthesis of metastable tetragonal zirconia by means of mechanochemical activation. *Applied Catalysis A: General* **227**, 299–307.
- Liu S, Qian X, Xiao J.** 2007. Synthesis and characterization of La<sub>0.8</sub>Sr<sub>0.2</sub>Co<sub>0.5</sub>Fe<sub>0.5</sub>O<sub>3-δ</sub> nanopowders by microwave assisted Sol-gel route. *Journal of Sol-Gel Science Technology* **44**, 187–193.
- Merino NA, Barbero BP, Ruiz P, Cadus LE.** 2006. Synthesis, characterization, catalytic activity and structural stability of LaCo<sub>1-y</sub>Fe<sub>y</sub>O<sub>3±λ</sub> perovskite catalysts for combustion of ethanol and propane. *Journal of Catalysis* **240**, 245–257.
- Mishra G, Tripathy M.** 1993. A critical review of the treatment for decolorization of textile effluent. *Colourage* **40**, 35-8.
- Nakamoto K.** 1978. *Infrared and Raman Spectra of Inorganic and Coordination Compounds*. Plenum Press, New York.
- Schaak RE, Mallouk TE.** 2002. Perovskite by design: a toolbox of solid-state reactions. *Chemistry Materials* **14**, 1455–1471.
- Siddique M, Farooq R, Khalid A, Farooq A, Mahmood Q, Farooq U, Raja IA, Shaukat SF.** 2009. Thermal-pressure-mediated hydrolysis of reactive blue 19 dye. *Journal of Hazardous Materials* **172**, 1007–1012.
- Sivaraj R, Namasivayam C, Kadirvelu K.** 2001. Orange peel as an adsorbent in the removal of acid violet 17 (acid dye) from aqueous solutions. *Waste Management* **21**, 105–110.

**Tejuca LG, Fiero JLG, ed.** 1993. Properties and applications of perovskite-type oxides. Marcel Dekker, New York.

**Temkin MJ, Pyzhev V.** 1940. Kinetics of ammonia synthesis on promoted iron catalysts. *Acta Physicochimica URSS* **12**, 217-222.

**Vijayaraghavan K, Padmesh TVN, Palanivelu K, Velan M.** 2006. Biosorption of nickel (II) ions onto *Sargassum wightii*: application of two-parameter and three parameter isotherm models. *Journal of Hazardous Materials B* **133**, 304-308.

**Wong Y, Yu J.** 1999. Laccase catalyzed decolorisation of synthetic dyes. *Water Research* **33**, 3512-20.

**Wu R, Qu J, He H, Yu Y.** 2004. Removal of azo dye Acid Red B (ARB) by adsorption and catalytic combustion using magnetic  $\text{CuFe}_2\text{O}_4$  powder. *Applied Catalysis B: Environmental* **48**, 49-56.

**Yazdanbakhsh M, Khosravi I, Goharshadi EK, Youssefi A.** 2010. Fabrication of nanospinel  $\text{ZnCr}_2\text{O}_4$  using sol-gel method and its application on removal of azo dye from aqueous solution. *Journal of Hazardous Materials* **184**, 684-689.